

# Inversion-free feedforward hysteresis control using Preisach model

Michael Ruderman

**Abstract**—We introduce a new inversion-free feedforward hysteresis control using the Preisach model. The feedforward scheme has a high-gain integral loop structure with Preisach hysteresis operator in negative feedback. This allows obtaining a dynamic quantity which corresponds to the inverse hysteresis output, as the loop error tends towards zero for a sufficiently high feedback gain. By analyzing the loop sensitivity function with hysteresis that acts as a state-varying phase lag, we demonstrate the achievable bandwidth and accuracy of the proposed control method. Remarkable fact is that the control bandwidth is theoretically infinite, provided the Preisach operator in feedback can be implemented in a way to ensure the  $C^0$  continuous hysteresis output. Numerical control examples with the Preisach hysteresis model in differential form are presented.

## I. INTRODUCTION

Hysteresis phenomena occur in quite different physical and technical systems, see e.g. [1], and often require an accurate compensation through dedicated control measures. From a system and control viewpoint, the hysteresis can be seen as a multi-valued quasi-static nonlinearity, affected by a nonlocal memory. The latter implies that some part of the history of previous states is retained and influences the current state of the system. Often, the hysteresis appears inside of more complex dynamic systems, so that the hysteresis output is not directly measurable for a feedback control. It appears, for example, with the magnetic flux density in controlled electromagnets or net electrical charge in piezoelectric actuators. For systems without hysteresis nonlinearity sensing, a pure feedforward control, correspondingly compensation, often seems preferable over some feedback control strategies.

In the control literature, a feedforward hysteresis control is mostly associated with constructing a model-based (sometimes also model-free) inverse (or its approximate) of the hysteresis. Some earlier works on controlling the unknown hysteresis go back e.g. to [2]. A more recent control framework with hysteresis compensation was also reported in [3]. Apart from that, a passivity-based stability and control of hysteresis were addressed, still in a feedback manner, in [4]. Another alternative compensation approach, which is worth to be mentioned here since addressing the relevant phase shift properties of a hysteresis system, was provided in [5]. A mixed recursive algorithm to control the output remnant of a hysteresis system was presented in [6]. An inverse multiplicative structure, that is relying on internal model-based principle, was shown in [7] with use of the Prandtl-Ishlinskii (see e.g. in [8]) hysteresis model in feedforwarding.

However, an artificial time-delay was necessary for bypassing an algebraic loop of the proposed scheme. Multiple works on hysteresis compensation with feedforward scheme have also been published in the context of inverse mapping, e.g. [9], or more generally inverse modeling of hysteresis systems to be controlled. Due to a variety of (often ad-hoc and approximative) approaches, and due to our focus on the Preisach [10] hysteresis model, we will only refer to some of them. The theoretical conditions for existence and properties of the inverse Preisach operator were known since [11]. However, to the best of the author's knowledge, no closed analytical form of the inverse Preisach operator suitable for feedforward control has been reported so far. A remarkably fast computation of the Preisach inverse, targeting the real-time implementation, was reported e.g. in [12] and in the multiple following works by the co-authors. The approach relies on the stored Everett functions and the so-called Preisach representation theorem, see [13] for detail. Different iterative inversion schemes, which are equally suitable for a real-time feedforwarding, were proposed, e.g. allowing also for an online adaptation in [14], and later in combination with an additional observation of the recent hysteresis state in [15]. The latter was also provided in a differential form, see the work [16], which is also used in the present contribution.

Differing from the approaches mentioned above, we propose a new type of the inversion-free feedforward hysteresis compensation. Because the proposed hysteresis control scheme is generic, and limited solely to the class of rate-independent hysteresis that can be captured by the Preisach operator, no specific application system is addressed explicitly. Notable possible applications, however, are in the operation of electromagnets, piezoelectric and magnetostrictive actuators, and other electro-magneto-mechanical devices with a rate-independent hysteresis in the input channel.

The rest of the paper is structured as follows. The basic problem formulation of a feedforward hysteresis compensation is given in section II. Here we also provide an approximate input-output view on the hysteresis behavior in terms of a harmonic response. In section III, the Preisach hysteresis operator is described, as far in detail as necessary, also in the differential form used in the proposed control scheme. The phase shift properties of the Preisach operator are elucidated based on the extreme case of a lumped two-point switching hysteresis. The proposed inversion-free hysteresis control scheme is introduced in section IV, together with analysis of the control errors and achievable performance. The numerical examples of compensating for one convex and one non-convex hysteresis are given in section V. The paper is concluded by a discussion provided in section VI.

M. Ruderman is with University of Agder, Department of Engineering Sciences, Norway. Email: michael.ruderman@uia.no  
Author's accepted manuscript, IEEE ECC2023

## II. FEEDFORWARD HYSTERESIS CONTROL

We consider a generic hysteresis system

$$y(t = \tau) = f[u(0 \leq t \leq \tau), y_0] \quad (1)$$

as a multi-valued nonlinear function  $f[\cdot]$ , which output at the time  $t = \tau$  depends on the recent and previous input values at  $t \leq \tau$  and the initial state  $y_0 \equiv y(t = 0)$ . Without loss of generality, we assume that  $u(t) \in \mathcal{C}^0$  and  $y(t)$  is almost always piecewise differentiable, except the reversal points where the  $\text{sign}(\dot{u})$  changes. In other words, we do not allow for stepwise inputs of hysteresis, while the input derivative does not have to be continuous with respect to time. Recall that for all input-output pairs  $(u, y)$ , cf. two examples in Fig. 2 (a) and (b), one can say the system (1) possesses memory since at any instant  $t$  the output  $y(t)$  is determined by the previous evolution of the input function  $u(t)$ , and not only the input value at the same time instant, cf. [8].

Now the objective is to design a controller, see Fig. 1, which will act as a feedforward hysteresis compensator and, therefore, guarantee for  $|y(t) - r(t)| < \varepsilon$ , where  $\varepsilon > 0$  is the smallest possible residual control error. In addition, a potentially large control bandwidth is required, that means  $\varepsilon(j\omega)$  remains upper bounded for a bounded angular frequency  $\omega < \omega_b$ . The design of a feedforward controller assumes that an accurate model of the hysteresis system is available, while we emphasize that the proposed controller is inversion-free, i.e. it does not require constructing or approximating the inverse of (1). Recall that a closed analytic form of the

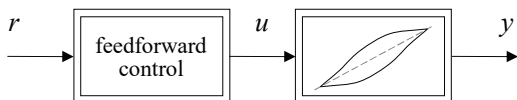


Fig. 1. Feedforward control of input-output hysteresis system

inverse of a multi-valued hysteresis function is not always available, like in case of the Preisach hysteresis operator. At the same time, feedforward hysteresis compensation may be required in several applications where a hysteresis output  $y$  appears rather as an internal state and is not available (or can not be used) during the controlled system operation.

As we focus on a rate-independent hysteresis in the strict sense (for definition and properties of rate-independence of hysteresis we refer to e.g. [8]), the output  $y$  depends on the sequence of the input values but not on the frequency with which they are proceeded. In other words, the rate-independent behavior of a hysteresis system is not influenced by any affine transformation on the time axis. It is also worth mentioning that a suitable scaling, correspondingly normalization, of the hysteresis input and output enables an assumption of the unity domain and range of (1), cf. Fig. 2. It means that a simple static mapping  $y(t) = u(t)$  would occur when there is no hysteresis. Considering two illustrative examples, depicted in Fig. 2 for a convex (a), (c) and non-convex (b), (d) hysteresis, one can recognize that the output exhibits a state-varying phase shift  $\phi(u(t))$

to a harmonic input process. As originated from an Ancient Greek word 'hysteresis', meaning 'lagging behind', the most of the phase shifts are of a lag type. That means, a time integral of the phase shift over a full period has always a negative sign. At the same time, a transient lead-type phase shift occurs for the non-convex hysteresis, cf. Fig. 2 (d).

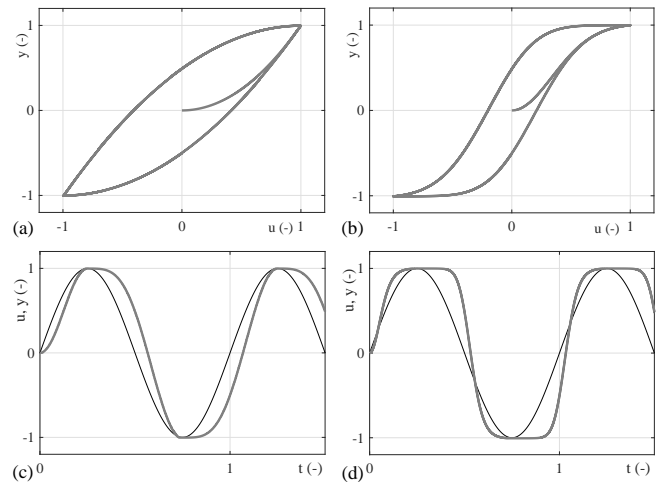


Fig. 2. Examples of a convex (a), (c) and non-convex (b), (d) hysteresis; black thin line of input and grey thick line of output in (c) and (d)

In order to analyze the input-output hysteresis properties, in a more familiar sense of the dynamic system, one can approximate the hysteresis output response to a harmonic input  $u(t) = \sin(\omega t)$  as follows

$$y(t) \approx \bar{y}(u_0, y_0) + A(u(t)) \sin(\omega t + \phi(u(t))). \quad (2)$$

The bias  $\bar{y}$  depends on the initial state of the hysteresis system and reveals, this way, a signature of a hysteresis memory. Generally, one can assume that  $\bar{y}$  is bounded by the main (major) loop of the hysteresis. Both, the gain factor  $A(\cdot)$  and phase shift  $\phi(\cdot)$  depend on the instantaneous hysteresis state, while  $|A| < \kappa < \infty$  and  $-\pi/2 < \phi < \pi/2$  can be assumed without loss of generality. The first assumption is because the bounded gain follows immediately from the Lipschitz-continuity of a hysteresis operator (1), cf. [8], while the corresponding Lipschitz constant is  $\kappa = \max \partial y / \partial u$ . The boundedness of the phase shift follows from the input-output behavior of an elementary hysteresis operator *hysteron*, as demonstrated below in section III.

Now we are in the position to introduce the feedforward control  $u(t) = g[r(t)]$ , so that its serial connection with a hysteresis system results in  $y = f[g[r], y_0] \rightarrow r$ . Before doing it in section IV, we will first describe the Preisach hysteresis operator, which is assumed for modeling the hysteresis system and used in the proposed control scheme.

## III. PREISACH HYSTERESIS OPERATOR

The scalar Preisach hysteresis model [10], [13] is one of the most powerful approaches for describing a multi-valued rate-independent hysteresis mapping in its proper sense. The Preisach hysteresis operator and its numerous

extensions have been used for several decades (see e.g. in [1]) in magnetism, material science, but also in the control and system engineering. We will briefly summarize the Preisach operator, as far as necessary for our developments, while we refer to the seminal literature [8], [13] for more fundamental and profound details on mathematical hysteresis operators.

The memory affected multi-valued static map of the Preisach hysteresis operator is given by

$$y(t) = H[u(t)] = \iint_{\alpha \geq \beta} \rho(\alpha, \beta) h(\alpha, \beta) [u(t)] d\alpha d\beta, \quad (3)$$

in which the elementary nonlinear operator  $h[\cdot]$  (also called *hysteron*) captures the spatially distributed internal state of the corresponding input-output system. The hysteron is nothing but an amplitude-delayed relay (see Fig. 4 on the left) which is parameterized by two threshold values  $\alpha \geq \beta$ . Upon passing the threshold values, the output of  $h[u]$  flips among the binary states  $+1$  (up state) and  $-1$  (down state), for  $u \geq \alpha$  and  $u \leq \beta$  correspondingly. For  $\beta < u(t) < \alpha$ , the hysteron keeps its previous binary state for  $\forall t > t_s$  where  $t_s$  is the time of the last flipping, i.e. switching at the threshold value. The entire Preisach operator is parameterized by the so-called Preisach density function  $\rho(\alpha, \beta)$ , which is defined over  $P = \{(\alpha, \beta) \mid \alpha \geq \beta\}$ . The most suitable geometrical interpretation of  $P$  and, correspondingly, state transitions of the Preisach hysteresis operator is by means of the Preisach plane (further denoted by  $P$ ). The plane is given in the relative  $(\alpha, \beta)$ -coordinates of the input domain, cf. Figs. 2 and 3. It is worth saying in advance that for a practical consideration and use of the Preisach hysteresis operator, both the domain and range of (3) are bounded, so that

$$u_{\min} \leq (\alpha, \beta) \leq u_{\max}$$

and

$$y_{\max} - y_{\min} = 2 \iint_P \rho(\alpha, \beta) d\alpha d\beta.$$

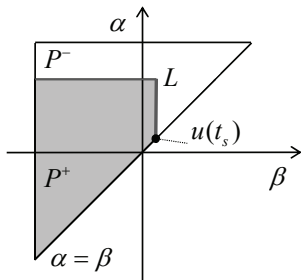


Fig. 3. Preisach plane with switching hysteresis state

At each time instant  $t$ , the Preisach plane is divided into two disjunct subsets, i.e.  $P(t) = P^+(t) \cup P^-(t)$ , which contain the hysterons in the 'up' state and 'down' state correspondingly. Both subsets are separated by a staircase interface  $L$ , cf. Fig. 3, which represents the instantaneous memory of the hysteresis system. The interface moves from bottom to top for  $\dot{u} > 0$  and from right to left for  $\dot{u} < 0$ ,

while the dynamic transformations of  $L$  occur by including the new local extrema and deleting the previous, according to the wiping-out hysteresis property, cf. [13].

One can easily show that

$$\begin{aligned} y(t) &= \iint_{P^+} \rho(\alpha, \beta) d\alpha d\beta - \iint_{P^-} \rho(\alpha, \beta) d\alpha d\beta = \\ &= \iint_P \rho(\alpha, \beta) d\alpha d\beta - 2 \iint_{P^-} \rho(\alpha, \beta) d\alpha d\beta, \end{aligned} \quad (4)$$

when considering, for instance, a decreasing input. Therefore, for two consecutive values  $u(t_2) < u(t_1)$  of a monotonically decreasing input  $\forall t_2 > t_1$ , the output difference can be obtained, from (4), as

$$\begin{aligned} \Delta y = y(t_2) - y(t_1) &= -2 \iint_{P^-(t_2)} \rho(\alpha, \beta) d\alpha d\beta + \\ &+ 2 \iint_{P^-(t_1)} \rho(\alpha, \beta) d\alpha d\beta = -2 \iint_{\Omega} \rho(\alpha, \beta) d\alpha d\beta. \end{aligned} \quad (5)$$

Here  $\Omega \equiv P^-(t_1) \setminus P^-(t_2)$  is the difference set of the switching region in  $P$ , i.e. where the hysterons flipped down during the time between  $t_1$  and  $t_2$ . Obviously, the switching region depends on  $\Delta u = u(t_2) - u(t_1)$ , and when taking the limiting value  $\lim \Delta u \rightarrow 0 \equiv du$  one can obtain, without loss of generality, the differential form of (3) as

$$dy = 2 \text{sign}(\dot{u}) \iint_{\Omega(du)} \rho(\alpha, \beta) d\alpha d\beta. \quad (6)$$

Note that at the switching time  $t_s$ , the set  $\Omega(du)$  coincides with the most bottom horizontal segment of  $L$  for  $\text{sign}(\dot{u}) = 1$  and with the most right vertical segment of  $L$  for  $\text{sign}(\dot{u}) = -1$ , both for a monotonically changing  $u(t)$ . If the input direction changes, i.e. the hysteresis operator experiences a local extremum, then  $\Omega(du) = L(u(t_s))$ , cf. Fig. 3. Integrating (6) with respect to  $y$ , one obtains the Preisach hysteresis output, provided the initial  $y(0)$  is known. More details on this differential form of the Preisach operator, also in the state-space formulation, can be found in [16].

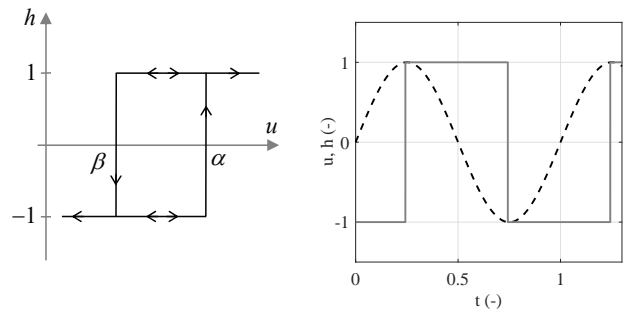


Fig. 4. Elementary hysteresis operator hysteron (on the left), and the corresponding input- and output-value harmonics (on the right)

Before introducing the hysteresis control, let us examine the phase shift characteristics of a hysteresis operator, cf. (2) and Fig. 2, based on the input-output behavior of a single hysteron depicted in Fig. 4. It is evident that the half of

period of the output level coincides with zero-crossing of the input harmonic. Furthermore, the output switching, where  $h$  crosses zero and has its zero-average, occurs at time instances of the input peaks. This provides exactly  $\pm\pi/2$  phase shift between the input and output harmonics of a hysteron, while the phase sign depends on the initial state of the hysteron i.e.  $h(t=0)$ . We also recall that the  $h$  hysteresis loop (as depicted in Fig. 4 on the left) represents a boundary case of the Preisach operator H, i.e. with a maximally possible loop area enclosed by the vertical hysteresis transitions at  $u_{\max}$  for 'up' and  $u_{\min}$  for 'down'. Note that within the  $P$  plane, this corresponds to the case when all hysterons are located in the left upper corner  $(\alpha, \beta) = (u_{\max}, u_{\min})$ . In general, closer the hysterons are located to the  $\alpha = \beta$  diagonal of the Preisach plane, lower phase shift is between the input  $u$  and corresponding output  $h$ . This allows concluding  $\max|\phi| = \pi/2$ , cf. section II and Figs. 2 and 4 (on the right).

#### IV. INVERSION-FREE HYSTERESIS CONTROL

The proposed inversion-free hysteresis control relies on an internal model principle and incorporates the high-gain integral feedback loop which aims controlling the hysteresis model  $\hat{f}[\cdot]$ , see Fig. 5. If the internal model control loop

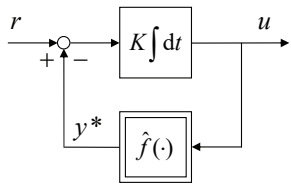


Fig. 5. Proposed feedforward hysteresis control  $u = g[r]$

achieves its goal, i.e. the modeled hysteresis output  $\hat{f} : u(t) \mapsto y^*(t)$  follows the reference  $r(t)$  as close as possible, then the output of the integral regulator, which is

$$u(t) = K \int (r(t) - y^*(t)) dt, \quad (7)$$

mimics the inverse of the hysteresis map i.e.  $\hat{f}^{-1} : y^*(t) \approx r(t) \mapsto u(t)$ . With this simple idea in mind, let us analyze the bandwidth and accuracy of the hysteresis controller  $u = g[r]$ , especially depending on the high-gain value  $K$ . Since we are eager to see how close the internally controlled  $y^*(t)$  value follows the reference  $r(t)$ , we consider the closed-loop error  $e = r - y^*$  as the principal measure of accuracy of the feedforward hysteresis compensator.

Let us first examine the linear case, i.e. without hysteresis, when a linear static mapping  $y^* = Au$  is in the closed-loop of the  $g$ -compensator. The loop error transfer function is

$$E_l(j\omega) = \frac{e(j\omega)}{r(j\omega)} = \frac{j\omega}{j\omega + KA}. \quad (8)$$

The above is a typical sensitivity function which drops towards zero as  $\omega \rightarrow 0$ . Note that the corner frequency  $(KA)$  can be shifted to the right by increasing the control gain  $K$ , provided the  $A$ -factor remains constant, cf. Fig. 6. When allowing for variations of  $A(\cdot)$ , that is unavoidable for

hysteresis nonlinearity, cf. (2), the feedback loop remains stable provided the static  $A \neq \text{const}$  nonlinearity satisfies the sector condition, cf. e.g. [17]. At the same time, the sensitivity function becomes degraded by the low bound  $A^- = \min(A)$ . This should be taken into account when designing  $K$ , while the upper bound  $A^+ = \max(A)$  expands the control bandwidth, cf. Fig. 6.

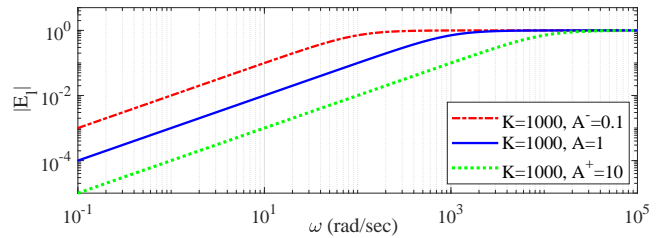


Fig. 6. Exemplary closed-loop error transfer function  $E_l$  for the control gain  $K = 1000$  and feedback variations:  $A^- = 0.1$ ,  $A = 1$ ,  $A^+ = 10$

Now, we expand our above consideration of the error transfer function to the case of approximating hysteresis in the loop, cf. (2) and Fig. 5. For the mostly occurring lag-type phase shift  $\phi$  (also most sensitive in terms of the stability), we consider a standard first-order lag transfer function

$$F(j\omega) = \frac{y^*(j\omega)}{u(j\omega)} = \frac{j\omega/(\delta\omega_0) + 1}{j\omega\delta/\omega_0 + 1}. \quad (9)$$

Two parameters,  $\omega_0$  and  $\delta$ , are characteristic for approximating the hysteresis response to a harmonic input. Obviously, due to the phase shift characteristics of interest, the angular frequency  $\omega_0$ , at which the phase lag is maximal, coincides with that of the harmonic input  $u(j\omega_0)$ . The factor  $\delta$  scales

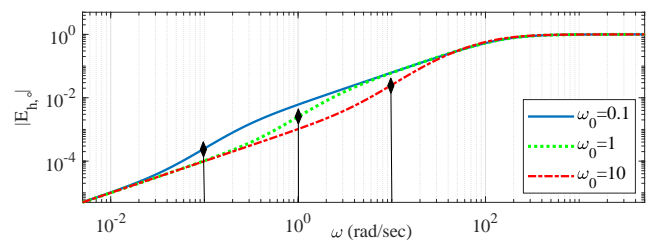


Fig. 7. Exemplary closed-loop error transfer function  $E_{h,\omega}$  for the assumed  $K = 1000$ ,  $A = 1$ , and  $\omega_0 = \{0.1, 1, 10\}$  rad/sec

the bandwidth of the lagging transfer characteristics around  $\omega_0$  and, thus, the phase-lag itself. For the transfer function (9), the phase lag is always  $-\pi/2 < \angle F(j\omega) < 0$ . And for an average phase lag  $\angle F(j\omega) = -\pi/4$ , which is sufficient for our qualitative analysis, the  $\delta = 2.5$  can be assumed in the following. Substituting the approximation (2) instead of  $\hat{f}(\cdot)$  into the closed control loop from Fig. 5, one obtains

$$e(j\omega) \left( 1 + \frac{KA}{j\omega} F(j\omega) \right) = r(j\omega) - \bar{y}. \quad (10)$$

It becomes evident that two transfer functions,  $E_{h,r}(j\omega) = e(j\omega)/r(j\omega)$  and  $E_{h,\bar{y}}(j\omega) = e(j\omega)/\bar{y}(j\omega)$ , can be considered and analyzed separately and in a similar manner. It is

also worth recalling that  $\bar{y}$  constitutes the bias depending on the hysteresis memory state, cf. (2). Therefore, only steady-state or low-frequency range, i.e.  $\omega \rightarrow 0$ , are relevant when analyzing  $E_{h,\bar{y}}(j\omega)$ . On the contrary, one is focusing on the frequency range around  $\omega = \omega_0$ , with a corresponding adjustment of the lag transfer function (9), when analyzing  $E_{h,r}(j\omega)$ . This refers to the reference input  $r(j\omega_0)$ . Assuming, as before, an exemplary control gain  $K = 1000$  and  $A = 1$ , the frequency response function of  $E_{h,o}$  is shown in Fig. 7 for  $\omega_0 = \{0.1, 1, 10\}$  rad/sec. Note that the analysis of  $E_{h,o}$  transfer function is equally valid in both cases  $o = r \vee \bar{y}$ . It is easy to see, from the labeled black vertical bars, how the closed-loop error changes depending on the angular frequency  $\omega_0$  of the reference signal. It can also be seen that for a steady-state bias, injected through  $\bar{y}$ , the closed-loop error goes to zero. Therefore, it becomes conclusive that with an increasing  $K$ -value, assigned with respect to  $A^-$  and  $A^+$  (both are known from the modeled hysteresis system), the same upper bound for  $|e|$  and, hence, for the hysteresis compensation error  $\varepsilon$ , can be guaranteed despite an increasing  $\omega_0$ . It implies, theoretically, an infinite control bandwidth, provided an infinite  $K$ -gain and an appropriate modeling of the hysteresis function  $\hat{f}$  are realizable.

## V. NUMERICAL EVALUATION

The proposed control is evaluated numerically together with the hysteresis system plant, both interconnected as depicted in Fig. 1. The simulated hysteresis system  $f[\cdot]$  and the one involved in the designed control, i.e.  $\hat{f}[\cdot]$ , use the same Preisach hysteresis operator in the differential form, see section III. The discrete  $(\beta, \alpha)$ -mesh of the  $400 \times 400$  size is assumed, that results in a total of 80200 hysterons, cf. [18]. Note that the allocated  $(\beta, \alpha)$ -matrix represents simultaneously the parameters space of the Preisach density function and the state-space of the binary hysterons. This allows for a memory- and computation-efficient implementation of the Preisach model, which is equally suitable for (and has been tested in) a real-time environment. Further details on the discretized real-time implementation in the differential form can be found in [15]. The high-gain of the internal model loop is assigned as  $K = 6000$ . This is done with respect to the input frequency, on the one hand, and the discretization level of the Preisach operator, on the other hand. Recall that the latter provokes a finite quantization of  $y$  and  $y^*$  and, thus, violates the theoretical assumption of the hysteresis output to be piecewise differentiable between two reversal points.

Two Preisach density functions depicted in Fig. 8 are exemplary taken for evaluation. The first one, shown in (a), is a uniform distribution of the hysterons with  $\rho(\alpha, \beta) = \text{const}$ . The second one, shown in (b), is a two-dimensional Gaussian normal distribution  $\mathcal{N}(\mu, \Sigma)$ , which is parameterized by the mean vector  $\mu$  and symmetric covariance matrix  $\Sigma$ , both in the relative  $(\alpha, \beta)$  coordinates. In both  $\rho$ -cases, the relative weights of the hysterons have been assumed so that the saturated hysteresis has the range  $y_{\min, \max} = \{-1, 1\}$ , while the input domain is considered to be of the same scale  $-1 \leq u \leq 1$ . Note that the uniform and Gaussian

normal Preisach density functions result in the hysteresis loops depicted in Fig. 2 (a) and (b), correspondingly.

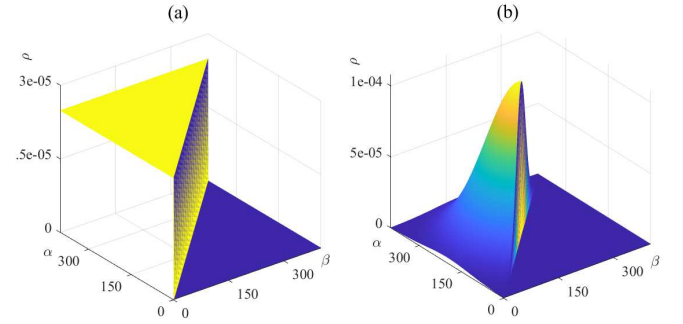


Fig. 8. Assumed Preisach density function over the discretized  $(\beta, \alpha)$  plane, (a) uniform distribution, (b) Gaussian normal distribution

First, a 'zigzag'-shaped input reference with a continuously increasing amplitude was applied for both Preisach density functions. This results in a set of continuously growing hysteresis loops, which are enveloped inside of each other. The produced control signal is shown in Fig. 9 in the

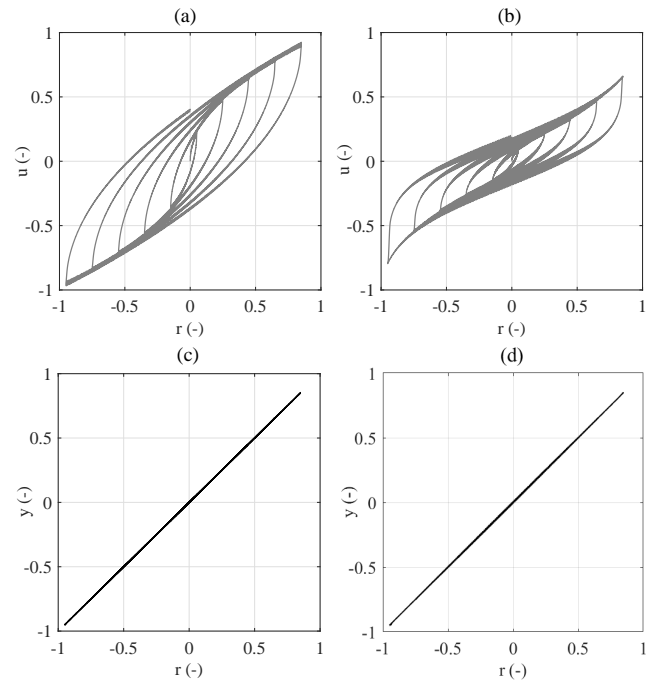


Fig. 9. Control over reference values (above) and output over reference values (below) of the hysteresis compensation for a zigzag shaped input, (a) and (c) uniform distribution, (b) and (d) Gaussian normal distribution

$(r, u)$  coordinates, for the uniform in (a) and for the Gaussian normal Preisach density function in (b), respectively. The compensated input-output behavior is shown in Fig. 9 in the  $(r, y)$  coordinates, in (c) and (d) correspondingly.

Next, a chirp reference input  $u = 0.9 \sin((2\pi\nu t)t)$ , was applied with a linearly progressing frequency  $\nu t$  between 0.1 and 10 Hz. Note that the reference amplitude was set to 0.9 for not reaching a fully saturated hysteresis state. The compensation results are shown in Fig. 10, for the uniform

Preisach density function on the left and for the Gaussian normal Preisach density function on the right. The hysteresis compensation error  $\varepsilon(\nu)$  is depicted as a function of the growing reference frequency in (a) and (b). The compensated input-output behavior is depicted in Fig. 10 in the  $(r, y)$  coordinates, in (c) and (d) correspondingly.

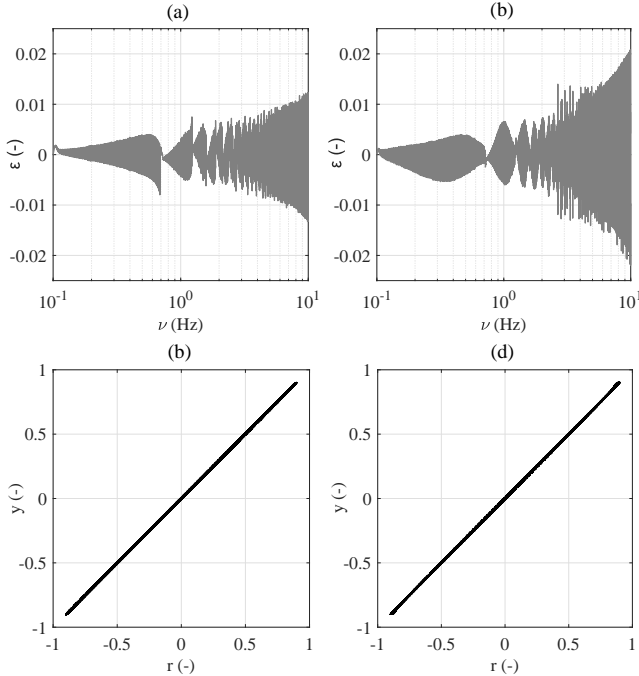


Fig. 10. Control error  $\varepsilon(\nu)$  (above) and output over reference values (below) of the hysteresis compensation for a 0.1-10 Hz chirp input, (a) and (c) uniform distribution, (b) and (d) Gaussian normal distribution

## VI. DISCUSSION

This paper proposed an inversion-free feedforward control of hysteresis systems, based on the internal model principle and Preisach operator of an arbitrary rate-independent hysteresis map. The Preisach model, which relies on a phenomenon-based weighted superposition of multiple elementary hysteresis operators *hysterons*, is the most flexible among the operator-based hysteresis models for shaping the hysteresis loops and the associated hysteresis memory. Although the existence of an inverse Preisach operator has been proven mathematically [11], there is no sound piecewise continuous and implementable analytical form for it up to now. Therefore, the proposed alternative inversion-free feedforward hysteresis compensator, which is based on the same standard Preisach operator, is advantageous. The single design parameter, apart from the identified Preisach model of the hysteresis system to be controlled, is the high-gain of an integral loop. For identification and adaptation of the Preisach hysteresis model itself, we refer to the lately proposed robust online estimator of the Preisach density function, see [18]. Since the high integral gain is used for an internal model control loop only and, thus, does not produce any saturated control actions, its value can be increased (at least theoretically) towards infinity. This results

in a theoretically *infinite bandwidth* of the compensator. This was analyzed in section IV and evaluated with numerical examples in section V. It was also shown that the upper bound of the residual control error is growing with 20 dB/dec in frequency domain of the reference input, cf. Figs. 7 and 10 (a) and (b). However, this fact represents a rather implementation- and application-related issue. Apart from a theoretically justified hysteresis compensation error, the residual error contents in  $\varepsilon(t)$  (propagated from  $e(t)$ ), are of a numerical nature owing to the discretized Preisach hysteresis operator. Justified, a finite  $(\alpha, \beta)$  mesh produces a quantized, to say 'staircase'-type, output  $y^*$  of the Preisach model. As this signal is fed back in a high-gain integral loop, the associated parasitic side-effects become visible in the resulted  $(r, u)$  mapping, cf. Fig. 9 (a), (b). A possible solution is increasing the size of  $(\alpha, \beta)$ -mesh with respect to  $\omega_0$  and  $K$ -gain values or using an  $y^*$ -interpolator.

## REFERENCES

- [1] G. Bertotti and I. D. Mayergoyz, *The Science of Hysteresis 1-3*, 1st ed. Academic Press, 2006.
- [2] G. Tao and P. V. Kokotovic, "Adaptive control of plants with unknown hysteresees," *IEEE Transactions on Automatic Control*, vol. 40, no. 2, pp. 200-212, 1995.
- [3] A. Esbrook, X. Tan, and H. K. Khalil, "Control of systems with hysteresis via servocompensation and its application to nanopositioning," *IEEE Transactions on Control Systems Technology*, vol. 21, no. 3, pp. 725-738, 2012.
- [4] R. B. Gorbet, K. A. Morris, and D. W. Wang, "Passivity-based stability and control of hysteresis in smart actuators," *IEEE Transactions on Control Systems Technology*, vol. 9, no. 1, pp. 5-16, 2001.
- [5] J. M. Cruz-Hernández and V. Hayward, "Phase control approach to hysteresis reduction," *IEEE transactions on Control Systems Technology*, vol. 9, no. 1, pp. 17-26, 2001.
- [6] M. Vasquez-Beltran, B. Jayawardhana, and R. Peletier, "Recursive algorithm for the control of output remnant of Preisach hysteresis operator," *IEEE Cont. Sys. Letters*, vol. 5, no. 3, pp. 1061-1066, 2020.
- [7] M. Al Janaideh, M. Rakotondrabe, I. Al-Darabsah, and O. Aljanaideh, "Internal model-based feedback control design for inversion-free feedforward rate-dependent hysteresis compensation of piezoelectric cantilever actuator," *Control Engin. Practice*, vol. 72, pp. 29-41, 2018.
- [8] A. Visintin, *Differential Models of Hysteresis*, 1st ed. Springer, 1994.
- [9] P. Krejci and K. Kuhnen, "Inverse control of systems with hysteresis and creep," *IEE Proceedings - Control Theory and Applications*, vol. 148, no. 3, pp. 185-192, 2001.
- [10] F. Preisach, "Ueber die magnetische Nachwirkung," *Zeitschrift Physik*, vol. 94, pp. 277-302, 1935.
- [11] M. Brokate and A. Visintin, "Properties of the Preisach model for hysteresis," *Journal für die reine und angewandte Mathematik (Crelles Journal)*, no. 402, pp. 1-40, 1989.
- [12] D. Davino, C. Natale, S. Pirozzi, and C. Visone, "A fast compensation algorithm for real-time control of magnetostrictive actuators," *Journal of Magnetism and Magnetic Materials*, vol. 290, pp. 1351-1354, 2005.
- [13] I. D. Mayergoyz, *Mathematical models of hysteresis and their application*, 2nd ed. Academic Press (imprint of Elsevier), 2003.
- [14] X. Tan and J. S. Baras, "Adaptive identification and control of hysteresis in smart materials," *IEEE Transactions on Automatic Control*, vol. 50, no. 6, pp. 827-839, 2005.
- [15] M. Ruderman and T. Bertram, "Discrete dynamic Preisach model for robust inverse control of hysteresis systems," in *IEEE 49th Conference on Decision and Control (CDC)*, 2010, pp. 3463-3468.
- [16] M. Ruderman, "State-space formulation of scalar Preisach hysteresis model for rapid computation in time domain," *Applied Mathematical Modelling*, vol. 40, no. 4, pp. 3451-3458, 2016.
- [17] H. Khalil, *Nonlinear Systems*, 3rd ed. Prentice Hall, 2002.
- [18] M. Ruderman and D. Rachinskii, "Discrete-time adaptive hysteresis filter for parallel computing and recursive identification of Preisach model," in *IEEE Conference on Control Technology and Applications (CCTA)*, 2018, pp. 1096-1101.